Applied Catalysis B: Environmental 132–133 (2013) 315–320

Contents lists available at SciVerse ScienceDirect

Applied Catalysis B: Environmental

journal homepage: www.elsevier.com/locate/apcatb

Water splitting from dye wastewater: A case study of BiOCl/copper(II) phthalocyanine composite photocatalyst

Ling Zhang, Wenzhong Wang*, Songmei Sun, Yuanyuan Sun, Erping Gao, Jie Xu

State Key Laboratory of High Performance Ceramics and Superfine Microstructures, Shanghai Institute of Ceramics, Chinese Academy of Sciences, 1295 Dingxi Road, Shanghai 200050, PR China

ARTICLE INFO

Article history:
Received 8 October 2012
Received in revised form
26 November 2012
Accepted 2 December 2012
Available online 10 December 2012

Keywords:
BiOCl
Copper phthalocyanine
Photocatalytic
Water splitting
Photosensitizer

ABSTRACT

Oxygen evolution is frequently the bottleneck determining the efficiency in the overall photocatalytic water splitting. Herein, for the first time overall water splitting reaction to H_2 and O_2 is realized on BiOCl/CuPc (copper phthalocyanine) composite from RhB (rhodamine B) solution under simulated solar light irradiation. The photosensitized RhB dye molecules supplied photo-generated holes which took part in the reaction of O_2 evolution. By loading CuPc, the efficiency of H_2 evolution is improved. On the base of the greatly enhanced photocurrent density, the considerable enhancement of performance can be attributed to the quick transfer of photogenerated electrons from the photosensitizer to the CB (conduction band) of BiOCl. Furthermore, as active electron traps, the oxygen vacancies on the surface of the BiOCl photocatalyst promote the separation efficiency of photo-generated electrons and holes, resulting in high photoactivity. This study presents a way that organic dye wastewater will be a useful system for the overall photocatalytic water splitting reaction to H_2 and O_2.

1. Introduction

Photocatalysis is becoming attractive because of the energy and environmental problems. From the view point of energy, photocatalysis could be used for splitting water, while for environment photocatalysis could be used for degrading organic pollutants. Both the photocatalytic water splitting and photocatalytic decomposition of pollutants are important ways for solar energy storage and conversion [1]. Though it is well known that dye molecules are good photosensitizer for photocatalysts and it has been proved they could improve the photocatalytic reaction rate efficiently [2,3], there are rare reports which combine the photocatalytic water splitting with the photocatalytic degradation of dye molecules in one reaction system. Considering the solar energy utilization and environment decontamination, production of hydrogen by photocatalytic water splitting from dye wastewater appears to be an exciting idea. In the present contribution we report that bismuth oxychloride/phthalocyanine copper (BiOCl/CuPc) composite photocatalyst is prepared by a simple methodology and an efficient photocatalytic system containing dye molecules is built for hydrogen and oxygen evolution.

As a photosensitizer, CuPc has intense absorption in the visible light region (600–800 nm) [4]. So, it could directly use solar light as an energy source. Furthermore, it is very stable in the photocatalytic process but some other dye photosensitizers themselves are often oxidized. As a co-photocatalyst, it could improve the spatial separation and enhance the lifetime of photogenerated carriers in a photocatalyst, thus increase the efficiency of photocatalysis. In the current study, CuPc is selected as a photosensitizer and a co-photocatalyst.

BiOCl, as one of the most important bismuth oxyhalides, has been proved as an effective photocatalyst for mineralization of organic compounds [5–7]. The layered structure of BiOCl can provide the space large enough to polarize the related atoms and orbitals. The induced dipole can separate the electron–hole pair efficiently and enhanced photocatalytic activity. Recently, Zan et al. reported that the low bond energy and long bond length of the Bi—O bond led to the production of oxygen vacancies on the BiOCl surface under UV light irradiation and resulted in higher photocatalytic activity [8]. On the other hand, the conduction band potential of BiOCl ($\sim E_{CB} = -1.1$ eV) is more negative than that of H^+/H_2 [9,10]. This indicates that it is possible for BiOCl photocatalyst to split water to produce H_2. However, bare BiOCl owns a broad band gap of about 3.2 eV, limiting its photocatalytic applications under solar light irradiation. Coupling with a photosensitizer will extend the light absorption of BiOCl to visible light region for the effective utilization of visible light (42% of the energy of the solar spectrum).

Herein, we report that BiOCl/CuPc photoelectrode shows an enhanced photocurrent density up to about 76 times higher than that of bare BiOCl electrode. We also found the photocatalysis mineralization capacity of BiOCl/CuPc is higher than that of BiOCl

* Corresponding author. Tel.: +86 21 5241 5295; fax: +86 21 5241 3122.
E-mail address: wzwang@mail.sic.ac.cn (W. Wang).

0926-3373/$ – see front matter © 2012 Elsevier B.V. All rights reserved.
http://dx.doi.org/10.1016/j.apcatb.2012.12.003

under Xe lamp irradiation. The overall water splitting reaction on BiOCl/CuPc was achieved in methanol–H_2O–RhB solution. The photocatalytic activity of O_2 evolution on BiOCl/CuPc photocatalyst can be enhanced in the acidic RhB dye solutions.

2. Experimental

2.1. Preparation of photocatalyst

The chemical reagents were purchased from Shanghai reagent Co. Ltd. (China). All the chemicals were used as received without further purification. In a typical experiment, 1.28 g of hexadecyltrimethylammonium chloride (CTAC), was dissolved in a mixed solution of 2-methoxyethanol (96 mL) and H_2O (4 mL). 1.94 g of $Bi(NO_3)_3{\cdot}5H_2O$ was added to 10 mL of ethylene glycol (EG) with stirring at room temperature. After $Bi(NO_3)_3$ was dissolved completely, it was added to the mixed solution with stirring. All the reactants were sealed in a flask and maintained at 120 °C for 5 h. For the BiOCl/CuPc sample, 0.005 g of CuPc dissolved in 10 mL of 2-methoxyethanol was added into the flask and the reaction system was heated at 120 °C for 1 h. After the reactions completed, a white (BiOCl) or blue (BiOCl/CuPc) precipitate was obtained, respectively. The precipitate was washed with deionized water and then dried at 60 °C for 12 h.

2.2. Characterization

The samples were characterized by X-ray powder diffraction (XRD) on a Rigaku powder diffractometer. Each sample was scanned using Cu Kα radiation with an operating voltage of 30 kV and an operating current of 100 mA. The scan rate of 4° min^{-1} was applied to record the patterns in the range of 10–80° at a step size of 0.01°. UV–vis diffuse reflectance spectra were recorded on an UV–vis spectrophotometer (Hitachi 3010) equipped with an integrating sphere. The Raman spectra were recorded on a JY HR-800 spectrometer provided by JY Company at room temperature with an excitation wavelength of 564 nm. In addition, a red LED lamp (3 W) with a wavelength of 620 nm was turned on in the measurement according to the experimental requirement.

2.3. Preparation of photocatalyst electrode

BiOCl and BiOCl/CuPc electrodes were prepared by electrophoretic deposition on fluorine-doped tin oxide (FTO) substrate [11,12]. The electrophoretic deposition was carried out in acetone solution (50 mL) containing iodine (10 mg) and photocatalysts powder (50 mg) which was dispersed by sonication for 3 min. The FTO electrodes (1.1 cm × 2 cm) was immersed in the acetone solution, parallel with the Pt electrode, and then bias of 10 V was applied for 3 min using a potentiostat. The photocatalyst-coated area was controlled to be ca. 1.1 cm × 1.5 cm. This procedure resulted in the formation of a photocatalyst film with relatively uniform thickness.

2.4. Photocatalytic reactions and photocurrent measurements

The photocatalytic water splitting reactions were carried out in a closed gas circulation and evacuation system. Typically, 0.2 g of photocatalyst was dispersed by a magnetic stirrer in H_2O solution containing 20% of CH_3OH in a reaction cell made of Pyrex glass. Rhodamine B (RhB) dye was added into this reaction system according to the experimental requirement. The suspension was then thoroughly degassed by N_2 and irradiated by a 500 W Xe lamp from the top of the reaction cell. The temperature of the reactant solution was maintained at 25 °C with cooling water during the reaction. The amount of evolved H_2 and O_2 was analyzed by an on-line gas chromatograph equipped with a transformation furnace detector.

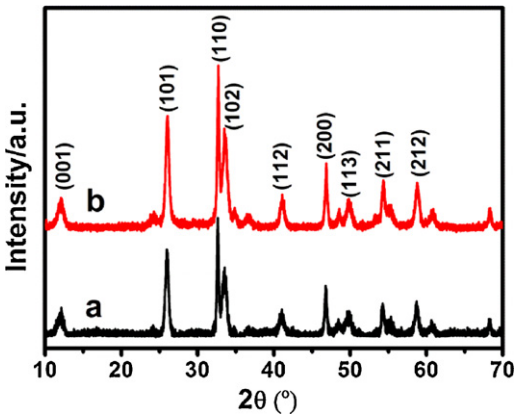

Fig. 1. XRD patterns of the BiOCl (a) and BiOCl/CuPc (b).

The photocatalytic activities in the mineralization of model pollutants of the as-prepared BiOCl and BiOCl/CuPc powders were evaluated by the degradation of RhB dye in an aqueous solution under different light irradiation. In a typical experiment, 0.1 g of the photocatalyst was dispersed in 100 mL of RhB (10^{-5} mol/L) solution. A 500 W Xe lamp and LED lamp (3 W) with a main emission wavelength of 400 nm and 620 nm were employed as light source in different experiments, respectively. At given time intervals, 5 mL of solution was collected from the suspension and immediately centrifuged, and the concentration of RhB after illumination was determined using an UV–vis spectrophotometer.

3. Results and discussion

3.1. Characterizations of BiOCl and BiOCl/CuPc photocatalyst

Fig. 1 shows the X-ray diffraction patterns of the bare BiOCl and BiOCl/CuPc samples. All diffraction peaks in Fig. 1a and b are identical to the structure of the tetragonal phase BiOCl (JCPDS card no. 06-0249). In addition, the intense peaks indicate the samples are well crystallized. Compared to the reference diffraction pattern (JCPDS, 06-0249), the diffraction peak intensity of the (1 1 0) plane is relatively higher than that of other planes. This probably relates to the growth orientation of the nanoplate (the SEM and TEM images of the as-synthesized sample shown in the supporting information).

Supplementary material related to this article found, in the online version, at http://dx.doi.org/10.1016/j.apcatb.2012.12.003.

The energy band structure feature of a semiconductor is one of the important factors determining its photocatalytic performance. Fig. 2 shows a comparison of UV–vis diffuse absorption spectra of as-prepared BiOCl and BiOCl/CuPc samples and their corresponding color. The absorption edges of both BiOCl and BiOCl/CuPc locate at about 350 nm, while the BiOCl/CuPc exhibited absorption bands in the wavelengths of 500–800 nm which could be attributed to the *Q*-band of CuPc. The *Q*-band corresponds to the π–π* transition of monomer from the HOMO to the LUMO of the Pc^{2-} ring. Furthermore, two splitting absorption bands were observed at around 610 and 700 nm, which was likely due to vibronic coupling in the excited state [13]. In addition, the band of 350–450 nm belongs to the typical B-band absorption of CuPc arising from the deeper π levels-LUMO transition. The above results indicated that the absorbance spectrum of BiOCl/CuPc was expanded to visible region after the CuPc loaded on the BiOCl photocatalyst.

Raman spectroscopy is a powerful technique for probing the vibrational and structural properties of crystals, measuring the symmetry of crystals, and investigating the stress state in the materials. Just as demonstrated by the XRD result, the BiOCl sample has

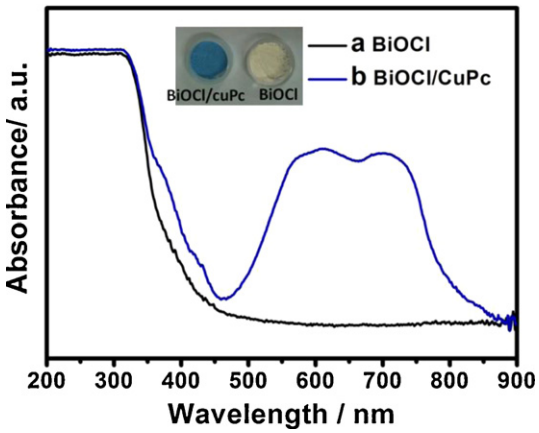

Fig. 2. UV–vis DRS of the BiOCl (a) and BiOCl/CuPc (b).

tetragonal structure which belongs to the *P*4/*nmm* space group with two molecular formulae per unit cell. For such structure, the correlation method of Fateley et al. indicates that the optical modes are as follows:

$$\Gamma = 2A_{1g} + 2A_{2u} + B_{1g} + 3E_g + 2E_u \quad (1)$$

where the g modes are Raman-active only and the u modes are infrared-active only. Fig. 3a and b shows the Raman spectra of the BiOCl and BiOCl/CuPc under different illumination. Usually, symmetric vibrations give rise to more intense Raman bands than asymmetric vibrations, the strong Raman band at 144.9 cm^{-1} and the band at 201.1 cm^{-1} are assigned to the A_{1g} and the E_g internal

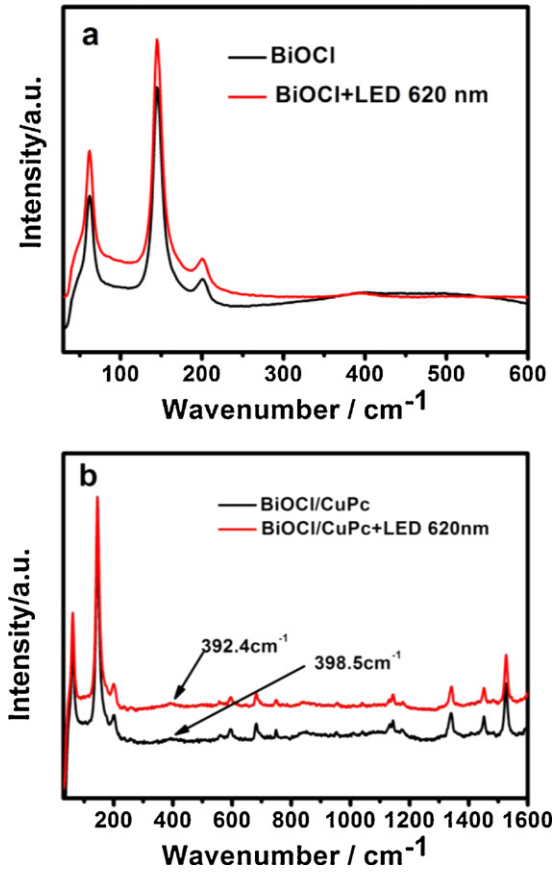

Fig. 3. Raman spectra of the BiOCl (a) and BiOCl/CuPc (b) under different laser irradiation.

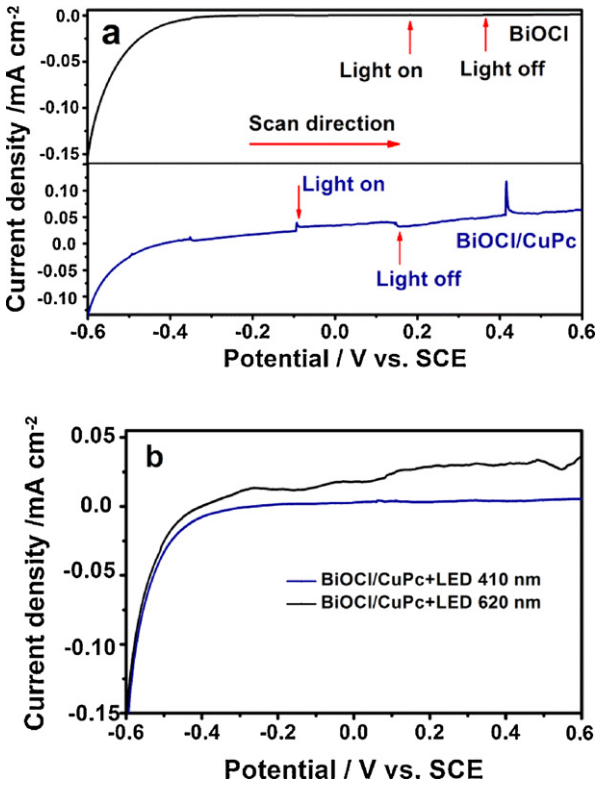

Fig. 4. Photocurrent measurement. (a) Photocurrent–potential characteristics of BiOCl and BiOCl/CuPc electrodes under Xe lamp irradiation (scan rate, 5 mV/s) with chopped light. (b) Photocurrent–potential characteristics of BiOCl/CuPc electrodes under different LED irradiation (scan rate, 5 mV/s). Electrolyte: 0.1 M pH 7.0 potassium phosphate buffer solution.

Bi–Cl stretching mode, respectively. For A_{1g} and E_g external modes of Bi–Cl, A_{1g} (60 cm^{-1}) is hard to be detected due to the limitation of the spectrophotometer and E_g is probably masked by the strong Raman band at 144.9 cm^{-1} [14]. Those vibrations were similar in the Raman spectra of the as-prepared BiOCl samples under the different illumination as shown in Fig. 3a. However, for the BiOCl/CuPc sample, the weak broad band (~398.5 cm^{-1}), which is assigned to the E_g and B_{1g} modes involving the motion of the oxygen atoms, shows blueshift of frequency to 392.4 cm^{-1} under the illumination of LED (620 nm) (Fig. 3b). This is attributed to the light-induced compressive stress in the BiOCl/CuPc. When the red light irradiated the BiOCl/CuPc powder, the photons could be absorbed by the CuPc. Then, the photogenerated electrons could transfer quickly to the CB of the BiOCl, which would cause the vibration of the local O atoms, thus leading to the compressive stress from the surrounding grains. Similar compressive stress-induced Raman shifts have been reported in other materials, e.g. BiOCl thin films [15] and single crystal ZnO [16].

3.2. Photocurrent density of BiOCl and BiOCl/CuPc photocatalyst

Fig. 4a shows current–voltage curves of as-prepared BiOCl and BiOCl/CuPc film electrodes under intermittent Xe lamp irradiation. Comparing to the BiOCl/CuPc film electrode, the photocurrent density of the BiOCl film electrode is very low. The maximum photocurrent density for the BiOCl/CuPc film electrode was 76 times higher than that of the bare BiOCl film electrode under Xe lamp irradiation. From Fig. 4b, we can found that the photocurrent density for the BiOCl/CuPc electrode, irradiated under the LED of 620 nm, was 142 times higher than that under the LED of 410 nm. It is estimated that the loading of CuPc on BiOCl significantly improve the photocurrent density of the electrode

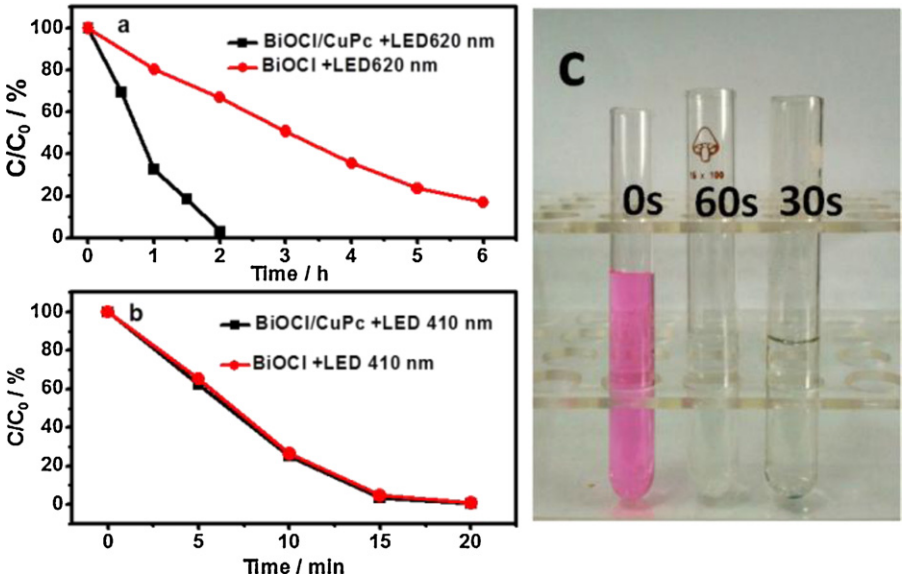

Fig. 5. The photocatalytic degradation of RhB under illumination of LED of 620 nm (a), LED of 410 nm (b), and (c) Xe lamp (recorded in photographs).

since the CuPc as a photosensitizer could response to the visible light from 500 to 800 nm. The photogenerated electrons were fast transferred from CuPc to the BiOCl and thus improved the photocurrent density.

3.3. Photocatalytic degradation of RhB on BiOCl and BiOCl/CuPc

The photocatalytic decomposition of RhB by using BiOCl and BiOCl/CuPc particles was investigated under different light irradiation. Fig. 5a displays the concentration C and initial concentration C_0 of RhB versus the degradation time under the irradiation of LED of 620 nm. It can be found that the RhB concentration decreased gradually with the increase of irradiation time. RhB was almost completely degraded after 2 h with the BiOCl/CuPc. Meanwhile, only 34% of RhB were degraded after 2 h with the BiOCl. In this system, CuPc has been suggested to react with pollutant by supplying electrons and generating CuPc$^{\bullet}$ radicals and active oxygen species ($^{\bullet}O_2$) that react with RhB to induce the degradation. In Fig. 5b, however, the RhB concentration decreased to nearly zero in 20 min under the irradiation of LED of 410 nm on both of BiOCl and BiOCl/CuPc. The photocatalytic decomposition process is quicker under the irradiation of LED of 410 nm than that of LED of 620 nm. It suggests that the photocatalytic activity of the BiOCl/CuPc was mainly resulted from the BiOCl, because the CuPc acted as a co-photocatalyst and responsed to visible light in the range of 500–800 nm. Fig. 5c showed that RhB molecules could be completely degraded within 60 s and 30 s for the BiOCl and BiOCl/CuPc samples under the irradiation of Xe lamp, respectively. The synergistic effect of co-catalysts and photosensitizer of CuPc is very favorable for the improvement of the photocatalytic activity in the mineralization of organic compound.

3.4. Photocatalytic H_2 evolution on BiOCl/CuPc in methanol–H_2O solution

There are rare reports that photocatalytic H_2 evolution on BiOCl in the literature though its conduction band is negative enough. Fig. 6 shows the temporal profile of H_2 evolution under simulated solar light irradiation (Xe lamp) on as-prepared BiOCl samples. For the sake of comparison we also load Pt on the BiOCl as reference. BiOCl, BiOCl/Pt and BiOCl/CuPc exhibit photocatalytic activity for H_2 generation under Xe lamp irradiation. The BiOCl/CuPc exhibited the highest activity of H_2 evolution among the samples. The mechanism of H_2 evolution operative in this system involves the injection of electrons from the excited state of the sensitizer into the conduction band of BiOCl leading to hydrogen evolution (Scheme 1). When the CuPc was excited by light illumination, the photogenerated electron from CuPc transferred into BiOCl while holes remained in the CuPc. It is worth to note that the oxygen vacancies on the surface of the BiOCl photocatalyst work as active electron trap to capture the electrons temporarily [6,8,17]. This process of charge separation is considered to be very fast, which electron injection from excited sensitizer into the semiconductor' conduction band occurs in less than 20 ps [2]. Therefore, direct electrons transfer from the excited photosensitizer to the BiOCl photocatalyst, which promote the separation efficiency of photogenerated electrons and holes, resulting in higher photoactivity.

In addition, a sacrificial electron donor, methanol in this system was employed to scavenge the photosensitizer's holes formed under illumination which prevent the recombination of the electron and hole. The above reasons could explain the hydrogen evolution in this reaction system.

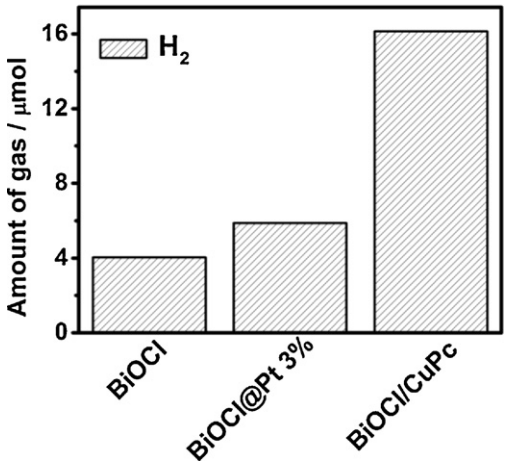

Fig. 6. Photocatalytic H_2 evolution on BiOCl and BiOCl/CuPc from H_2O/MeOH (20%, v/v). *Reaction conditions*: 0.2 g of catalyst; water/MeOH (200 mL); light source, Xe lamp (500 W); reaction time, 4 h.

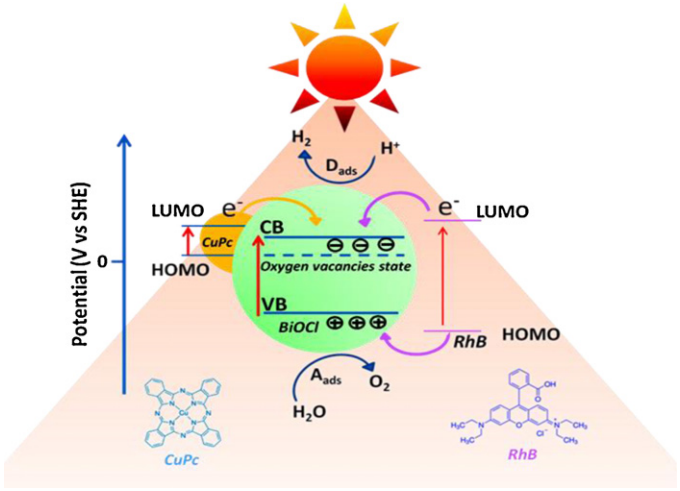

Scheme 1. A proposed mechanism of photocatalytic water splitting using BiOCl/CuPc under simulated sunlight irradiation.

3.5. Overall water splitting on BiOCl/CuPc in methanol–H_2O–RhB solution

Oxygen evolution is frequently the bottleneck determining the overall efficiency in the overall photocatalytic water splitting because the activation energy for the oxidation reaction for O_2 production is much higher than that of H_2 production [18]. In contrast to the simplicity of hydrogen generation, formation of oxygen from water is an uphill reaction involved a four-electron transfer process. So the research on the photocatalytic oxygen evolution has recently been intensified as it serves as the key step for the artificial water oxidation.

Here, the overall water splitting was realized in a methanol–H_2O–RhB system although the activity for overall water splitting is still low. In Fig. 7, a few of O_2 was detected in the methanol–H_2O system. However, when the RhB and methanol were involved in the reaction system at the same time, more O_2 evolution was observed. Furthermore, the H_2O–RhB system has higher activity of O_2 evolution but no H_2 was detected when sacrificial electron donor absent in the reaction solution. It was also found that the amount of O_2 produced in the acidic medium was more than that in the basic medium. We observed that, under the irradiation of the UV–vis light, the RhB molecules were easy to be degraded at acidic pH, but they were very stable in the basic medium. It means the O_2 evolution rate is relative high with the degradation of the RhB molecules. The faster decomposition of the RhB molecules is, the more O_2 produced. We proposed that RhB dye molecules worked as a "sacrificial photosensitizer" in this system. Under Xe lamp irradiation, RhB adsorbed on the surface of BiOCl was photosensitized. Photo-generated electron (from LUMO) can transfer to the BiOCl semiconductor since the LUMO levels of RhB is more negative than the CB edge potential of BiOCl. At the same time, the photosensitizer's holes formed on illumination would not only decompose RhB itself, but also take part in the reaction of O_2 evolution, because the HOMO levels of RhB is more positive than the VB edge potential of BiOCl [19,20]. On the other hand, if methanol and OH^-, as sacrificial electron donor, were employed to scavenge the holes, which would delay decomposition rate of the RhB molecules and thus reduce the production of O_2.

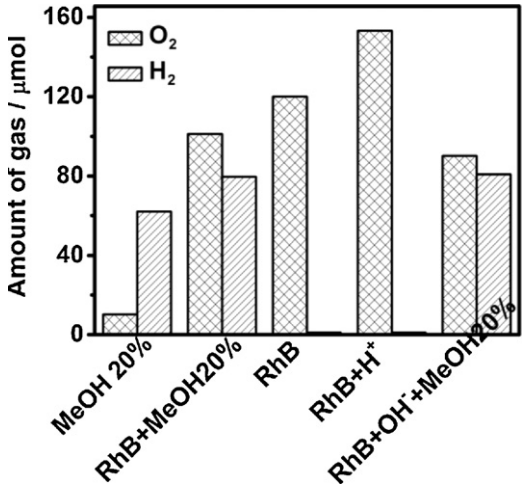

Fig. 7. Photocatalytic water splitting on BiOCl and BiOCl/CuPc under different conditions. *Reaction conditions*: 0.2 g of catalyst; light source, Xe lamp (500 W); reaction time, 1 h.

4. Conclusion

We demonstrated that the copper phthalocyanine as a photosensitization loading on BiOCl can improve photocatalytic activity. The enhancement of photocatalytic activity and photocurrent density can be attributed to the photosensitization which injected electrons from the excited state of the sensitizer into the conduction band of BiOCl. We also found the photocatalytic decomposition of dye molecules in the aqueous solution has an essential relation with the photocatalytic activity of O_2 evolution. The photosensitizer's holes formed on the RhB supplied more holes to take part in the reaction of O_2 evolution. By taking the advantages of dye waste decontamination, the overall water splitting reaction achieved on BiOCl/CuPc photocatalyst in the dye wastewater system is a prospective method for solar energy storage and conversion.

Acknowledgements

This work was supported by the National Natural Science Foundation of China (50902144, 51272303 and 51272269), 973 Program (2013CB933203) and Science Foundation for Youth Scholar of State Key Laboratory of High Performance Ceramics and Superfine Microstructures (SKL 200904).

References

[1] M.D. Hernández-Alonso, F. Fresno, S. Suárez, J.M. Coronado, Energy & Environmental Science 2 (2009) 1231–1257.
[2] A. Nada, H. Hamed, M. Barakat, N. Mohamed, T. Veziroglu, International Journal of Hydrogen Energy 33 (2008) 3264–3269.
[3] C. Chen, W. Ma, J. Zhao, Chemical Society Reviews 39 (2010) 4206–4219.
[4] M. Zhang, C. Shao, Z. Guo, Z. Zhang, J. Mu, T. Cao, Y. Liu, ACS Applied Materials & Interfaces 3 (2011) 369–377.
[5] X. Chang, J. Huang, C. Cheng, Q. Sui, W. Sha, G. Ji, S. Deng, G. Yu, Catalysis Communications 11 (2010) 460–464.
[6] L. Ye, L. Zan, L. Tian, T. Peng, J. Zhang, Chemical Communications 47 (2011) 6951–6953.
[7] J. Jiang, K. Zhao, X. Xiao, L. Zhang, Journal of the American Chemical Society 134 (2012) 4473–4476.
[8] L. Ye, K. Deng, F. Xu, L. Tian, T. Peng, L. Zan, Physical Chemistry Chemical Physics 14 (2012) 82.
[9] S.Y. Chai, Y.J. Kim, M.H. Jung, A.K. Chakraborty, D. Jung, W.I. Lee, Journal of Catalysis 262 (2009) 144–149.
[10] L. Ye, C. Gong, J. Liu, L. Tian, T. Peng, K. Deng, L. Zan, Journal of Materials Chemistry 22 (2012) 8354–8360.
[11] D. Wang, R. Li, J. Zhu, J. Shi, J. Han, X. Zong, C. Li, Journal of Physical Chemistry C 116 (2012) 5082–5089.
[12] T. Ohno, L. Bai, T. Hisatomi, K. Maeda, K. Domen, Journal of the American Chemical Society 134 (2012) 8254–8259.
[13] Z. Guo, C. Shao, M. Zhang, J. Mu, Z. Zhang, P. Zhang, B. Chen, Y. Liu, Journal of Materials Chemistry 21 (2011) 12083–12088.

[14] Y. Tian, C.F. Guo, Y. Guo, Q. Wang, Q. Liu, Applied Surface Science 258 (2012) 1949–1954.
[15] S. Cao, C. Guo, Y. Lv, Y. Guo, Q. Liu, Nanotechnology 20 (2009) 275702.
[16] T.S. Jeong, M.S. Han, C.J. Youn, Y.S. Park, Journal of Applied Physics 96 (2004) 175.
[17] X. Zhang, L. Zhao, C. Fan, Z. Liang, P. Han, Computation Materials Science 61 (2012) 180–184.
[18] A. Primo, T. Marino, A. Corma, R. Molinari, H. Garcia, Journal of the American Chemical Society 133 (2011) 6930–6933.
[19] X. Chang, M.A. Gondal, A.A. Al-Saadi, M.A. Ali, H. Shen, Q. Zhou, J. Zhang, M. Du, Y. Liu, G. Ji, Journal of Colloid and Interface Science 377 (2012) 291–298.
[20] T.B. Li, G. Chen, C. Zhou, Z.Y. Shen, R.C. Jin, J.X. Sun, Dalton Transactions 40 (2011) 6751–6758.